T1-weighted MRI images accurately represent the volume and surface of architectural mineral damage of osteonecrosis of the femoral head: comparison with high-resolution computed tomography.

Tristan Pascart, Julien Paccou, Thomas Colard, Laurène Norberciak, Julien Girard, Jérôme Delattre, Pierre Marchandise, Julie Legrand, Guillaume Penel, Raphaël Coursier, et al.

T1-weighted MRI images accurately represent the volume and surface of architectural mineral damage of osteonecrosis of the femoral head: comparison with high-resolution computed tomography

Tristan Pascart,MD,PhD[1;2], Julien Paccou,MD,PhD [2;3], Thomas Colard,DDS,PhD[2], Laurène Norberciak[4],BSc, Julien Girard,MD,PhD [5], Jerôme Delattre[2], BSc, Pierre Marchandise[2], BSc, Julie Legrand,MD[6], Guillaume Penel,DDS,PhD[2], Raphaël Coursier,MD,PhD [7], Sophie Putman,MD[5], Bernard Cortet,MD,PhD [2;3], Greet Kerckhofs,PhD*[8;9;10], Jean-François Budzik,MD,PhD *[2;6].

*equal contribution

1 Department of Rheumatology, Lille Catholic Hospitals, University of Lille, F-59160 Lomme, France

2 EA 4490, PMOI, Physiopathologie des Maladies Osseuses Inflammatoires, University of Lille, F-59000, Lille, France

3 Department of Rheumatology, Hopital Salengro, Centre Hospitalier Universitaire de Lille, University of Lille, F-59000, Lille, France

4 Department of Medical Research, Biostatistics, Lille Catholic Hospitals, University of Lille, F-59160, Lomme, France

5 Department of Orthopaedic Surgery, Hopital Salengro, Centre Hospitalier Universitaire de Lille, F-59037, Lille, France

6 Department of Radiology, Lille Catholic Hospitals, University of Lille, F-59160 Lomme, France

7 Department of Orthopaedic Surgery, Lille Catholic Hospitals, University of Lille, F-59160 Lomme, France

8 Skeletal Biology and Engineering Research Center, Department of Development and Regeneration, KU Leuven, Leuven, Belgium

9 Prometheus - Division of Skeletal Tissue Engineering Leuven, KU Leuven, Leuven, Belgium.

10 Biomechanics lab, Institute of Mechanics, Materials, and Civil Engineering, UCLouvain, Louvain-la-Neuve, Belgium.

Corresponding author: Tristan Pascart _ Pascart.tristan@ghicl.net – Laboratoire Physiopathologie des Maladies Osseuses Inflammatoires – EA 4490 – Faculté de Chirurgie Dentaire - Place de Verdun – 59000 Lille - +33320167946

Article type : Original article

Running Head: MRI and HRμCT assessment of osteonecrosis

Word count: 3201

Type of manuscript: original article

Abstract

The potency of magnetic resonance imaging (MRI) to measure the exact extent of osteonecrosis of the femoral head (ONFH) remains uncertain. The objective of this study was to determine if the volume of necrosis assessed with MRI accurately reflects the volume of architectural mineral alterations in osteonecrosis of the femoral head by comparison with high-resolution microfocus X-ray computed tomography (HR-μCT). Fourteen male patients aged 53 years [46.2;59.0] suffering from ONFH were prospectively enrolled to undergo preoperative MRI and ex vivo analysis using HR-μCT. The necrotic zone on T1-weighted MRI scans was defined as total necrosis (delimited by the low-signal peripheral band) or dark necrosis (low-signal lesions only). The HR-μCT scans delimited outer necrosis and inner necrosis by including or excluding the sclerotic zone. The intra-class correlation coefficient (ICC) was calculated to compare the agreement of surface areas and volumes of necrosis measurements with the two techniques. There was an overall excellent agreement between MRI dark necrosis volume and HR-μCT outer necrosis volume (ICC=0.91[0.54;0.98]) while the MRI total necrosis volume showed poor agreement with both HR-μCT delimitations of necrosis volume. For surface area, agreement between MRI dark necrosis and HR-μCT delimitations was good for inner necrosis (ICC=0.70[0.21;0.9]) and moderate for outer necrosis (ICC=0.58[0.07;0.85]).

This study demonstrates that measurement of the MRI lesions provides a reliable assessment of the extent of ONFH-related architectural damage.

Key Words: osteonecrosis; femur head necrosis; X-ray microtomography; magnetic resonance imaging

1. Introduction

Osteonecrosis of the femoral head (ONFH) is a debilitating disease resulting from necrosis and eventual collapse of the femoral head [1]. It is estimated that 5 to 12% of the 500,000 annual hip replacements performed in the United States are due to ONFH [2]. Assessing the extent of the femoral necrotic zone is a challenge for the classification, prognosis and discussion of therapeutic options for the management of ONFH [3]. So far, calculating Koo's angle (modified Kerboul's angle [4]) on magnetic resonance imaging (MRI) acquisitions is one of the main references in routine practice [5] as Koo and Kim had shown that the extent of osteonecrosis was predictive of future collapse [6] (Supplementary Figure).

A precise assessment of the volume (and surface area) of the necrosis has an impact on the range of procedures that can be considered. Indeed, conservative options rather than radical total hip arthroplasty can be attempted in some cases. The success of hip resurfacing and core decompression, for instance, is conditioned by the localization and extent of the necrosis [7-10]. Volume evaluation of the necrotic zone remains imperfect to date and is consequently underused to the benefit of old qualitative classifications [11-13].

MRI is the most sensitive and precise imaging technique to identify and delineate necrosis available in clinical practice. However, modifications of the MRI signal in routine sequences only provide an assessment of the medullar alterations occurring during ONFH, and not the alterations of the mineral trabeculae that are responsible for the defective femoral biomechanical properties involved in the collapse of the femoral head. Histopathologic studies have been performed to examine the significance of MRI observations of ONFH in terms of actual extent of tissue necrosis and tend to conclude that there is an imperfect correlation between histological findings and MRI readings [8]. *Ex vivo* studies showed that the volume of ONFH measured by MRI T1-weighted images may not accurately reflect the extent of histological lesions [14].

High-resolution microfocus X-ray computed tomography (HR-μCT) allows the detection of changes in the structure of mineralized tissue with a significantly higher spatial resolution than standard μCT [15, 16]. In ONFH, a previous μCT study with similar spatial resolution described the architectural alterations of trabeculae in the necrotic and sclerotic zones while the trabecular architecture was preserved in the non-necrotic parts of the femoral head [17].

The objective of this study was to verify whether MRI-assessed necrosis volume and surface area accurately reflect HR-μCT-determined volume and surface area of architectural mineral alterations in ONFH.

2. Methods

This study investigates a diagnostic tool (MRI) with a level I-II evidence.

2.1.Ethics approval and registration

The study was approved by the French national board (CPP Nord-Ouest 03/018/2015) and by the French drugs and health products agency (reference B-151581-32). The ClinicalTrials registration number is NCT02733900.

2.2.Patients

Patients suffering from ONFH staged Ficat 3 or 4 [18] and requiring total hip replacement were prospectively enrolled in the study from April 2016 to September 2017. ONFH was secondary to corticosteroid treatment[19], excessive alcohol intake[19] or idiopathic. Demographic data were collected at the inclusion visit, together with the history of the disease, alcohol intake, corticosteroid use, and any history of fracture. Patients provided written informed consent to

undergo a dedicated MRI scan at a maximum 6 weeks prior to surgery and accepted to donate their femoral head to be scanned with HR-µCT.

2.3.MRI scans

2.3.1. MRI Acquisitions

All exams were performed on a 1.5T MRI scan (MR 450W Gem, General Electrics, Milwaukee, Illinois, USA). Patients were examined in supine position. A phased-array body coil covered the pelvis.

Routine MR sequences were used. According to our routine clinical protocol, a 3D T1-weighted sequence with isotropic voxels was used (DISCO: DIfferential Subsampling with Cartesian Ordering). T1-weighted sequences were used to confirm the diagnosis of ONFH, by identifying a thick continuous hypointense line that joins subchondral bone on two points in a given imaging plane. T1-weighted sequence parameters were as follows: 3D acquisition was performed in the axial plane; field of view was 410 x 410mm; matrix was 352 x 350mm; pixel size was 1.2 x 1.3mm; slice thickness was 1.6mm; reconstructed voxel size was 1.2 x 1.2 x 1.2mm; 256 slices were acquired; time of repetition was 450ms; time of echo was defined as "minimum"; bandwidth was 62.5 Hertz; K-space parallel imaging was used (autocalibrating reconstruction for cartesian imaging, ARC) with a factor of 2; acquisition time was 4min 45sec.

2.3.2 Measurements of MRI volumes

Slice-by-slice delimitation of the necrotic zone and of the whole femoral head was performed manually using Slicer 3D 4.6 software (www.slicer.org) [20, 21]. If the area of necrosis gave a heterogeneous signal (low and isosignal zones associated on the T1-weighted sequence), two zones of necrosis were determined. The first was delineated by the peripheral low signal band (without taking into account the signal of the content of the necrotic zone) and was named MRI total necrosis. The second included only the zone in low signal and was named MRI dark necrosis (Figure 1). Three volumes were calculated by the software: total necrosis

volume (TNV, mm^3), dark necrosis volume (DNV, mm^3) and femoral head total volume (FHTV, mm^3) (Figure 1). The percentage of necrosis affecting the femoral head was determined using Koo's method [6].

Surface areas were calculated with the software Avizo Fire 8.1 (FEI, Berlin, Germany) from the surface intersection of the reconstructed volumes of the entire femoral head and the necrosis (both TNV and DNV). Intersection of the volumes of necrosis and of the femoral head provided the surface area of the femoral head affected with osteonecrosis as well as the proportion of the surface of the femoral head affected with necrosis. Three surface areas were determined: the femoral head total surface area (FHTS, mm^2), the dark necrosis surface area (DNS, mm^2) and the total necrosis surface area (TNS, mm^2).

2.4.*HR*-µ*CT*

2.4.1 Image acquisition

Femoral heads were immediately frozen at -80°C following surgery. HR-µCT image acquisition was performed on the frozen samples using the following scan parameters to obtain the highest possible spatial resolution (30 µm voxel size) and sufficient image quality in the shortest scanning time possible: 60kV, 650µA, 500ms exposure time, image skip 0, frame averaging 1, 1800 images over 360°. A 0.5 mm filter of aluminum was used to reduce beam hardening during the acquisition. These acquisition settings resulted in a 15-min scanning time per sample. We used a Phoenix NanoTom M (GE Measurement and Control Solutions, Germany) for the image acquisition. During reconstruction (Datos|x, GE Measurement and Control Solutions), we applied a beam hardening correction of 7 and a Gaussian filter of 3.

2.4.2. HR-µCT image processing and analysis

Images of femoral heads were first reoriented according to their anatomical positions using DataViewer software (Bruker Micro CT, Belgium) allowing for a coronal observation of the necrosis to facilitate its delimitation. Images were treated to reduce the noise and the range of shades of grey to isolate the mineral bone with the following processing steps: gaussian filtering, multilevel thresholding (Otsu method, 3D, thresholding level 2), global thresholding, and sweep despeckle.

Regions of interest (ROIs) were determined manually every 50 cross-sections using CT Analyzer 1.17.7.2 software (Bruker micro CT, Belgium). The ROIs were manually delineated independently by two readers were interpolated by the software resulting in a volume of interest (VOI). The necrotic zone was determined in two ways, first by including the sclerosis surrounding the necrotic area (outer limit of necrosis) or excluding it (inner limit of necrosis). The subchondral boundary of inner necrosis was defined by the last visible microcrack identified as an interruption of the subchondral plate. The femoral head was visually delimited at the femoral neck by the threshold between subchondral and cortical bone. Volumes and surface areas of inner and outer necrosis and of the entire femoral head were obtained from the 3D dataset using Avizo Fire 8.1.

Figure 1 provides an illustration of ROI determination for both HR-µCT and MRI.

2.5.*Statistical analysis*

All statistical analyses were performed using R version 3.4.2. Qualitative variables are described by numbers and frequencies; quantitative variables by the median and interquartile interval because of the small sample size.

The Chi-square test or Fisher's exact test as appropriate, was used for comparative analysis of proportions between groups. Continuous variables were compared using the Mann-Whitney-Wilcoxon test.

Inter-observer agreement of the volumes measured with HR-µCT was assessed both for inner and outer limit by computing the intra-class correlation coefficient (ICC) and its 95% confidence interval.

Irr package (R software) was used taking into account a model with two random factors, with estimates of agreement on the raw data. The agreement was considered very good if the ICC was greater than 0.8 strictly, good if the ICC was between 0.61 and 0.8, moderate if the ICC was between 0.6 and 0.41, and bad otherwise.

The volumes of necrosis measured by MRI and HR-µCT were compared. First, the agreement was assessed by the ICC as described above. Complementarily, the Spearman coefficient correlation and its 95% confidence interval were calculated as well as the relative difference between the measures of both examinations. The correlation was considered in the same way as the ICC. The same calculations were performed for surface areas.

Significance level was set at 5%.

3. Results

3.1.Patients

A total of 14 male patients, median age 53 years [46.2;59.0] (ranging from 39.3 to 65.8 years old), were included in the study. The Ficat classification was 3 for five patients and 4 for nine patients. The cause of ONFH was active or past excessive alcohol intake for 8 patients and corticosteroid treatment for 3 patients. The diagnosis of idiopathic ONFH was retained for 3

patients. The diagnosis of ONFH was made 6 months [4; 13] before surgery. The values of volumes and surface areas of ONFH measured using the two imaging techniques are detailed in Table 1. The median MRI DNV and TNV were 16642 mm^3 [10618;20757] and 22062 mm^3 [13970;29096] respectively. According to Koo's angle, necrosis affected 42% [35 ; 52] of the femoral head. The median HR-µCT volumes of inner and outer necrosis were 12955 mm^3 [8442;14524] and 19451 mm^3 [13314;21519] respectively.

3.2.Inter-reader agreement for HR-µCT volume

Inter-reader agreement for the delimitation of inner and outer necrotic zones on HR-µCT images was excellent. For the volume of inner necrosis, the ICC was 1 [0.99;1], for the outer delimitation including the sclerotic zone the ICC was 0.98 [0.94 ; 0.99].

3.3.MRI and HR-µCT ONFH volume by delimitation

Agreement between the two techniques was excellent only between MRI DNV and HR-µCT outer necrosis volume: ICC = 0.91 [0.54;0.98].

MRI DNV overestimated HR-µCT inner necrosis volume by 29% [20.8%; 34.2%] leading to a poorer agreement between the two volume assessments (ICC = 0.6 [0 ; 0.89]), but the correlation ρ was excellent (0.89 [0.60;0.99]) because the volume overestimation was systematically made in the same proportion. MRI TNV exhibited very poor to moderate agreement and correlation with both HR-µCT delimitations of necrosis (Table 2). The scatter plots illustrate these findings as agreement between volume assessments increased with the proximity of the linear regression line with the diagonal line. Correlation on the other hand increased with the closeness of dots with the linear regression line (Figure 2).

The proportion of femoral head affected by necrosis estimated by Koo's angle showed very poor agreement with the proportion of necrosis defined by HR-µCT as inner necrosis (ICC = 0.07 [0;0.41]) or outer necrosis (ICC = 0.17 [0;0.6]). Correlation was poor with HR-µCT inner necrosis (ρ = 0.35 [-0.3;0.7]) and outer necrosis (ρ = 0.31 [-0.29;0.75]). Koo's angle assessment of the proportion of necrosis agreed very well with MRI TNV (ICC = 0.74 [0.36;0.91]), but poorly with MRI DNV (ICC = 0.24 [0; 0.64]).

3.4.Area of the femoral head surface affected with ONFH according to MRI and HR-µCT

Measurement of the total surface area of the femoral head affected by necrosis, i.e. MRI TNS, showed moderate agreement with HR-µCT inner necrosis (ICC = 0.55 [0.04;0.84]) and outer necrosis (ICC = 0.53 [0;0.84]). Correlation was good between MRI TNS and HR-µCT inner necrosis (ρ = 0.67 [0.05;0.97]) and moderate with outer necrosis (ρ = 0.55 [-0.09;0.94]). Agreement between MRI DNS and HR-µCT was good for inner necrosis (ICC = 0.70 [0.21;0.9]) and moderate for outer necrosis (ICC = 0.58 [0.07;0.85]). Correlation was very good between MRI DNS and HR-µCT for inner necrosis (ρ = 0.85 [0.54;0.97]) and good for outer necrosis (ρ = 0.78 [0.28;0.96]).

3.5.Proportion of the full femoral head surface affected by ONFH assessed by MRI and HR-µCT

In order to overcome partial volume effects, which have an impact on surface measurements, the proportions of the full femoral head surface affected by necrosis, as determined by the two imaging techniques, were assessed. Agreements, correlations and median differences reported in Table 3 were similar for MRI and HR-µCT measurements.

Figure 3 illustrates the superimposition of MRI necrosis volume on HR-µCT 3D rendering, highlighting the accurate MRI delineation of subchondral plate fractures in the femoral head surface, including the sclerotic zone in the trabeculae.

4. Discussion

This study demonstrates that the low signal lesions in T1-weighted MRI images can provide a reliable assessment of the extent of the architectural mineral damage during ONFH. More precisely, T1-weighted DNV reflects the extent of ONFH volume and encompass the cicatricial sclerotic zone which was not known so far. MRI DNS accurately delimits the surface of the femoral head presenting subchondral microcracks. Importantly, non-hypointense T1-weighted necrotic lesions, that were historically considered to be 'mummified necrosis', do not relate to any architectural modifications.

Our findings show that the necrotic lesions seen on T1-weighted images as hyperintense signals do not correspond to any alteration in the architectural mineral structure. Indeed, within the necrotic zone, bone marrow T1-weighted signals can be as hyperintense as "normal" bone marrow outside the necrotic zone. In the literature, these T1-weighted hyperintense lesions are commonly described as 'mummified' zones of necrosis [22]. Our study suggests that these "mummified" zones are not related to mineral architecture alterations and presumably would have preserved biomechanical properties. These results contradict those of Hu et al., who found similar volumes between medical CT and MRI images despite the fact that the study also included ONFH with heterogenous T1-weighted signals [23].

Accurately defining the extent of ONFH is more than an intellectual challenge since the result has significant clinical relevance. At a time when conservative techniques are being developed, it is essential to determine which zones of bone tissue can be preserved during the surgical procedure. For instance for hip resurfacing, the appropriateness of the procedure

depends greatly on the extent of subchondral cracks, information that can be provided by preoperative MRI [24]. Our study highlights the fact that the modified Kerboul's angle (Koo's angle) does not provide an appropriate assessment of the degree architectural necrotic damage in cases more severe than the pre-collapse stage [6].

In our study, the surface of the femoral head with subchondral cracks was accurately delimited by the low signal lesions in the T1-weighted MRI images. Hamada et al. demonstrated that subchondral fractures were within the zone delineated by the sclerotic zone, which seemed to be the starting point of the fracture [25]. We further support these results by superimposing MRI images on micro-CT 3D reconstructions in which microcracks of the subchondral plate appeared in the zone delineated by the peripheral sclerotic bone (Figure 3). Subchondral plate cracks were only present in the zone defined by the T1-weighted low signal zone. This suggests that physicians could rely on T1-weighted MRI images and should expect that subchondral bone is preserved beyond the low signal zone although these subchondral fractures are not visualized by MRI [26].

MRI not only assesses the extent of medullar lesions, but also reflects the architectural mineral damage that has more clinical biomechanical relevance. Prior studies compared the volumes of ONFH measured with MRI to macroscopic and histological measures of femoral heads slices [14, 27]. MRI, macroscopy and histology overall provided good but uneven correlations of volumes of ONFH depending on the considered zone of the femoral head. None of them addressed the fundamental issue of mineralized trabecular and subchondral damage, which is responsible for the biomechanical properties of bone. Hu et al. addressed this issue by comparing MRI images to those obtained with conventional CT and macroscopical examinations of femoral heads. With a limited spatial resolution inherent to medical CTs, the study also suggested that MRI and CT provided volumes of ONFH similar to the one found on macroscopic observations of bone samples, but could not provide data on the sclerotic zone nor

the extent of subchondral cracks [23, 28]. Our results support the hypothesis that trabecular architectural damage only occurs around the bone marrow depleted of its fatty content, now replaced by necrotic tissue. Kishida et al. suggested that the T1-weighted low signal peripheral band corresponds to the cicatricial sclerotic zone [14]. The resolution of the HR-µCT images in our study suggests that this sclerotic zone is wider and that the low signal band more likely designates the periphery of this sclerotic zone.

This study has some limitations. First, all cases were end-stage ONFH needing prosthetic replacement so these findings may not be extrapolated to early stages of ONFH. It is however noteworthy that what marked the disease of our participants, for whom the diagnosis of ONFH had been made only a few months before surgery, was more its severity than its duration. Exploring early necrosis cases will require advanced imaging techniques capable of simultaneously assessing bone marrow modifications, architectural damage and bone mechanical properties. Dual-energy and particularly spectral CTs will aid in that prospect, and experimental MRI sequences such as UltraShort TE sequences or -processing techniques such as texture analysis may allow to precisely assess the architectural damage together with the bone marrow edema non-invasively [29-31]. Second, inclusions were limited to frequent causes of ONFH in men, so the results may not be applicable to other causes of ONFH and do not explore potential gender disparities. Third, the large differences in spatial resolution obtained with MRI and HR-µCT could have an important influence on the raw measurements mainly for surface areas of ONFH [32]. To reduce this effect, we also compared the ratio of ONFH surface area to the total surface of the femoral head determined with the two imaging techniques. The raw data produced similar findings suggesting that the partial volume effect had a non-significant impact on surface area comparisons. Finally, sample size was relatively small, though sufficient to identify the MRI and HR-µCT couple with the best agreement and correlation. Yet, the confidence intervals of agreements and correlations were wide, ranging in

most cases from low or intermediate values thus decreasing the strengths of the results, even when intra-class correlation coefficients were high in average.

5. Conclusions

Although ONFH is defined as the volume that is limited by a T1-weighted hypointense line on MRI scans whatever the signal of the necrosis, our study shows that this volume covers both normal and abnormal mineral architecture, as identified on HR-μCT. Mineral architecture alterations correspond to the low signal lesions in the T1-weighted hypointense zones. Further research on ONFH must consider this point, especially in the perspective of conservative treatments assessment.

Acknowledgements

We acknowledge the valuable technical support from the Department of Medical Research of the Lille Catholic Hospitals, especially Dr Amélie Lansiaux, Mrs Domitille Tristram, Mrs Melody Plets and Mrs Justine Monvoisin.

This work was funded by the Lille Catholic University federative fund. GK was financed by a postdoctoral grant and a travel grant of the Research Foundation - Flanders (FWO/12R4315N and FWO/V415416N). The high-resolution microCT images were generated at the X-ray computed tomography facility of the Department of Development and Regeneration of the KU Leuven, financed by the Hercules Foundation (project AKUL 13/47).

Conflict of interest disclosure

No benefits in any form have been received or will be received from a commercial party related directly or indirectly to the subject of this article.

Contributions

TP, GK and JFB participated to the conception and design of the study, acquisition of data, analysis and interpretation of data, drafted the article or revised it critically for important intellectual content and gave their final approval of the version to be submitted

JP, TC, JD, JL, PM, BC, GP, RC, SP, JG participated to the acquisition and interpretation of data, revised the manuscript critically and approved the final version of the manuscript.

References

[1] M.A. Mont, J.J. Cherian, R.J. Sierra, L.C. Jones, J.R. Lieberman, Nontraumatic Osteonecrosis of the Femoral Head: Where Do We Stand Today? A Ten-Year Update, J Bone Joint Surg Am 97(19) (2015) 1604-27.
[2] C.G. Zalavras, J.R. Lieberman, Osteonecrosis of the femoral head: evaluation and treatment, J Am Acad Orthop Surg 22(7) (2014) 455-64.
[3] M.E. Steinberg, G.D. Hayken, D.R. Steinberg, A quantitative system for staging avascular necrosis, J Bone Joint Surg Br 77(1) (1995) 34-41.
[4] M. Kerboul, J. Thomine, M. Postel, R. Merle d'Aubigne, The conservative surgical treatment of idiopathic aseptic necrosis of the femoral head, J Bone Joint Surg Br 56(2) (1974) 291-6.
[5] D.R. Steinberg, M.E. Steinberg, J.P. Garino, M. Dalinka, J.K. Udupa, Determining lesion size in osteonecrosis of the femoral head, J Bone Joint Surg Am 88 Suppl 3 (2006) 27-34.
[6] K.H. Koo, R. Kim, Quantifying the extent of osteonecrosis of the femoral head. A new method using MRI, J Bone Joint Surg Br 77(6) (1995) 875-80.
[7] C.L. Tai, Y.C. Chen, P.H. Hsieh, The effects of necrotic lesion size and orientation of the femoral component on stress alterations in the proximal femur in hip resurfacing - a finite element simulation, BMC Musculoskelet Disord 15 (2014) 262.
[8] F. Sadile, A. Bernasconi, F. Carbone, F. Lintz, G. Mansueto, Histological fibrosis may predict the failure of core decompression in the treatment of osteonecrosis of the femoral head, Int J Surg 44 (2017) 303-308.
[9] S. Nakasone, M. Takao, T. Sakai, T. Nishii, N. Sugano, Does the extent of osteonecrosis affect the survival of hip resurfacing?, Clin Orthop Relat Res 471(6) (2013) 1926-34.
[10] B. Mazieres, F. Marin, P. Chiron, L. Moulinier, J.M. Amigues, M. Laroche, A. Cantagrel, Influence of the volume of osteonecrosis on the outcome of core decompression of the femoral head, Ann Rheum Dis 56(12) (1997) 747-50.
[11] G.C. Lee, M.E. Steinberg, Are we evaluating osteonecrosis adequately?, Int Orthop 36(12) (2012) 2433-9.

[12] K. Takashima, T. Sakai, H. Hamada, M. Takao, N. Sugano, Which Classification System Is Most Useful for Classifying Osteonecrosis of the Femoral Head?, Clin Orthop Relat Res 476(6) (2018) 1240-1249.
[13] M.J. Grecula, CORR Insights(R): Which Classification System Is Most Useful for Classifying Osteonecrosis of the Femoral Head?, Clin Orthop Relat Res 476(6) (2018) 1250-1252.
[14] Y. Kishida, T. Nishii, N. Sugano, K. Nakanishi, T. Sakai, H. Miki, T. Ochi, H. Yoshikawa, Measurement of lesion area and volume by three-dimensional spoiled gradient-echo MR imaging in osteonecrosis of the femoral head, J Orthop Res 21(5) (2003) 850-8.
[15] G. Kerckhofs, M. Durand, R. Vangoitsenhoven, C. Marin, B. Van der Schueren, G. Carmeliet, F.P. Luyten, L. Geris, K. Vandamme, Changes in bone macro- and microstructure in diabetic obese mice revealed by high resolution microfocus X-ray computed tomography, Sci Rep 6 (2016) 35517.
[16] C. Wang, X. Wang, X.L. Xu, X.L. Yuan, W.L. Gou, A.Y. Wang, Q.Y. Guo, J. Peng, S.B. Lu, Bone microstructure and regional distribution of osteoblast and osteoclast activity in the osteonecrotic femoral head, PLoS One 9(5) (2014) e96361.
[17] J.X. Ma, W.W. He, J. Zhao, M.J. Kuang, H.H. Bai, L. Sun, B. Lu, A.X. Tian, Y. Wang, B.C. Dong, Y. Wang, X.L. Ma, Bone Microarchitecture and Biomechanics of the Necrotic Femoral Head, Sci Rep 7(1) (2017) 13345.
[18] R.P. Ficat, Idiopathic bone necrosis of the femoral head. Early diagnosis and treatment, J Bone Joint Surg Br 67(1) (1985) 3-9.
[19] B.H. Yoon, L.C. Jones, C.H. Chen, E.Y. Cheng, Q. Cui, W. Drescher, W. Fukushima, V. Gangji, S.B. Goodman, Y.C. Ha, P. Hernigou, M. Hungerford, R. Iorio, W.L. Jo, V. Khanduja, H. Kim, S.Y. Kim, T.Y. Kim, H.Y. Lee, M.S. Lee, Y.K. Lee, Y.J. Lee, M.A. Mont, T. Sakai, N. Sugano, M. Takao, T. Yamamoto, K.H. Koo, Etiologic Classification Criteria of ARCO on Femoral Head Osteonecrosis Part 1: Glucocorticoid-Associated Osteonecrosis, J Arthroplasty 34(1) (2019) 163-168 e1.
[20] Y.M. Kim, J.H. Ahn, H.S. Kang, H.J. Kim, Estimation of the extent of osteonecrosis of the femoral head using MRI, J Bone Joint Surg Br 80(6) (1998) 954-8.
[21] M.E. Steinberg, S.C. Oh, V. Khoury, J.K. Udupa, D.R. Steinberg, Lesion size measurement in femoral head necrosis, Int Orthop (2018).
[22] L.W. Bassett, J.M. Mirra, A. Cracchiolo, 3rd, R.H. Gold, Ischemic necrosis of the femoral head. Correlation of magnetic resonance imaging and histologic sections, Clin Orthop Relat Res (223) (1987) 181-7.
[23] L.B. Hu, Z.G. Huang, H.Y. Wei, W. Wang, A. Ren, Y.Y. Xu, Osteonecrosis of the femoral head: using CT, MRI and gross specimen to characterize the location, shape and size of the lesion, Br J Radiol 88(1046) (2015) 20140508.
[24] M.P. Revell, C.W. McBryde, S. Bhatnagar, P.B. Pynsent, R.B. Treacy, Metal-on-metal hip resurfacing in osteonecrosis of the femoral head, J Bone Joint Surg Am 88 Suppl 3 (2006) 98-103.
[25] H. Hamada, M. Takao, T. Sakai, N. Sugano, Subchondral fracture begins from the bone resorption area in osteonecrosis of the femoral head: a micro-computerised tomography study, Int Orthop 42(7) (2018) 1479-1484.
[26] A.R. Kolb, J.M. Patsch, W.D. Vogl, E. Benca, D. Stelzeneder, R. Windhager, J.G. Hofstaetter, The role of the subchondral layer in osteonecrosis of the femoral head: analysis based on HR-QCT in comparison to MRI findings, Acta Radiol (2018) 284185118786070.
[27] P. Hernigou, J.C. Lambotte, Volumetric analysis of osteonecrosis of the femur. Anatomical correlation using MRI, J Bone Joint Surg Br 83(5) (2001) 672-5.
[28] O.O. Aruwajoye, M.K. Patel, M.R. Allen, D.B. Burr, P.B. Aswath, H.K. Kim, Microcrack density and nanomechanical properties in the subchondral region of the immature piglet femoral head following ischemic osteonecrosis, Bone 52(2) (2013) 632-9.
[29] C.H. Suh, S.J. Yun, W. Jin, S.H. Lee, S.Y. Park, C.W. Ryu, Diagnostic performance of dual-energy CT for the detection of bone marrow oedema: a systematic review and meta-analysis, Eur Radiol 28(10) (2018) 4182-4194.

[30] A. Nazaran, M. Carl, Y. Ma, S. Jerban, Y. Zhu, X. Lu, J. Du, E.Y. Chang, Three-dimensional adiabatic inversion recovery prepared ultrashort echo time cones (3D IR-UTE-Cones) imaging of cortical bone in the hip, Magn Reson Imaging 44 (2017) 60-64.
[31] W.C. Bae, P.C. Chen, C.B. Chung, K. Masuda, D. D'Lima, J. Du, Quantitative ultrashort echo time (UTE) MRI of human cortical bone: correlation with porosity and biomechanical properties, J Bone Miner Res 27(4) (2012) 848-57.
[32] M.A. Gonzalez Ballester, A.P. Zisserman, M. Brady, Estimation of the partial volume effect in MRI, Med Image Anal 6(4) (2002) 389-405.

Tables and figures legends

Table 1. Median volumes and surface areas of necrosis and femoral heads measured with T1-weighted MRI and HR-µCT and their ratios.

	Median [Q1-Q3]
Volumes	
% of the femoral affected with ONFH according to Koo's angle (Kerboul modified)	42 [35 ; 52]
MRI femoral head total volume (mm^3)	47250 [43179 ; 52265]
MRI total necrosis volume (mm^3)	22062 [13970 ; 29096]
MRI dark necrosis volume (mm^3)	16642 [10618 ; 20757]
Volume ratio MRI total necrosis volume/femoral head (%)	49 [32 ; 53]
Volume ratio necrosis MRI dark necrosis volume/femoral head (%)	32 [24 ; 47]
HR-µCT volume of the femoral head (mm^3)	50734 [46203 ; 55000]
HR-µCT volume of outer necrosis (mm^3)	19451 [13314 ; 21519]
HR-µCT volume of inner necrosis (mm^3)	12955 [8442 ; 14524]
Volume ratio HR-µCT outer necrosis/femoral head (%)	38 [26 ; 47]
Volume ratio HR-µCT inner necrosis/femoral head (%)	23 [17 ; 29]
Surfaces	
MRI femoral head total surface area (mm^2)	8780 [8191 ; 9566]
MRI total necrosis surface area (mm^2)	2654 [1599 ; 3062]
MRI dark necrosis surface area (mm^2)	2240 [1432 ; 2833]
Surface ratio MRI total necrosis/femoral head (%)	31 [18 ; 35]
Surface ratio MRI dark necrosis/femoral head (%)	22 [15 ; 33]
HR-µCT surface of the femoral head (mm^2)	8804 [8027 ; 10059]
HR-µCT surface of outer necrosis (mm^2)	2681 [2048 ; 2909]
HR-µCT surface of inner necrosis (mm^2)	1748 [1349 ; 2369]
Surface area ratio HR-µCT outer necrosis/femoral head (%)	18 [17 ; 26]
Surface area ratio HR-µCT inner necrosis/femoral head (%)	26 [24 ; 31]

Table 2. Agreement (intra-class correlation coefficient ICC and its 95% confidence interval), correlation (Spearman's correlation coefficient ρ and its 95% confidence interval) and median relative differences between measurements of the volume of osteonecrosis measured with T1-weighted MRI and HR-µCT.

Compared volumes of necrosis	**ICC [CI 95%]**	**ρ [CI 95%]**	**Median relative difference [Q1-Q3]** (reference=MRI)
HR-µCT inner necrosis - MRI dark necrosis	0.6 [0 ; 0.89]	0.89 [0.6 ; 0.99]	-29% [-34.2% ; -20.8%]
HR-µCT inner necrosis - MRI total necrosis	0.19 [0 ; 0.57]	0.45 [-0.21 ; 0.85]	-33.2% [-52.7% ; -25.9%]
HR-µCT outer necrosis - MRI dark necrosis	0.91 [0.54 ; 0.98]	0.89 [0.57 ; 1]	16.5% [3.4% ; 24.1%]
HR-µCT outer necrosis - MRI total necrosis	0.48 [0 ; 0.79]	0.56 [-0.08 ; 0.93]	1.7% [-28.5% ; 20.8%]

Table 3. Agreement (intra-class correlation coefficient ICC and its 95% confidence interval), correlation (Spearman correlation coefficient ρ and its 95% confidence interval) and median relative differences between measurements of the surface ratio of osteonecrosis on the full femoral head measured with magnetic resonance imaging (MRI) and high-resolution microfocus X-ray computed tomography (HR-µCT).

Compared surface ratio necrosis/full femoral head	**ICC [CI 95%]**	**ρ [CI 95%]**	**Median relative difference [Q1-Q3]** (reference=MRI)
HR-µCT inner necrosis - MRI dark necrosis	0.49 [0 ; 0.82]	0.64 [0.03 ; 0.98]	-20.8% [-43.6% ; -3.8%]
HR-µCT inner necrosis - MRI total necrosis	0.56 [0 ; 0.85]	0.55 [-0.12 ; 0.87]	-0.3% [-22.7% ; 33.7%]
HR-µCT outer necrosis - MRI dark necrosis	0.74 [0.31 ; 0.92]	0.81 [0.45 ; 0.96]	-12% [-28.2% ; 11.7%]
HR-µCT inner necrosis - MRI total necrosis	0.76 [0.36 ; 0.92]	0.71 [0.32 ; 0.88]	9.3% [-2.2% ; 35.4%]

Figure 1. Definition of necrotic zones on MRI and high-resolution microCT scans. Definition of necrotic zones on T1-weighted MRI scans with A. heterogeneous lesions of a right femoral head with B. delineation with of the total necrosis and C. the dark necrosis only in a 62 year-old patient with right osteonecrosis of the femoral head. D. Native T1-weighted MRI scans of a left ONFH with E. delineation of necrosis and F. subsequent volume 3D reconstruction from coronal slices, and G. microCT image of osteonecrosis, H. binarized microCT images and I. delineation of inner (red) and outer (green) necrosis on the microCT section of a left femoral head from a 51 year-old patient.

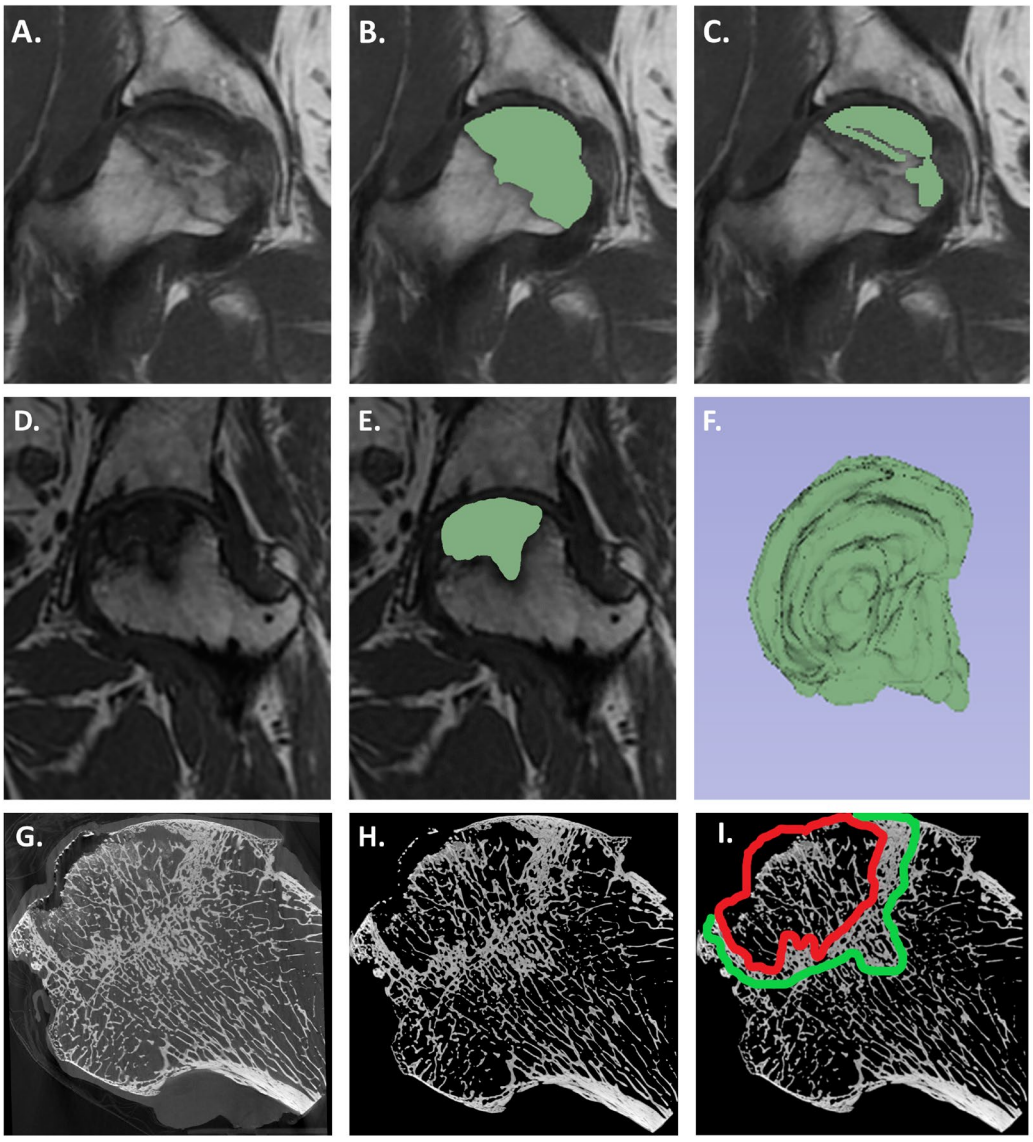

Figure 2. Scatter plots of the volume measurements of necrosis with MRI and HR- µCT. A. MRI dark necrosis and HR-µCT inner necrosis (R^2 0.87), B. MRI total necrosis and HR-µCT inner necrosis (R^2 0.89), C. MRI dark necrosis and HR-µCT outer necrosis (R^2 0.25), D. MRI total necrosis and HR-µCT outer necrosis (R^2 0.34). The linear regression line (correlation) appears in full black and the diagonal line (perfect agreement) appears in dotted-line.

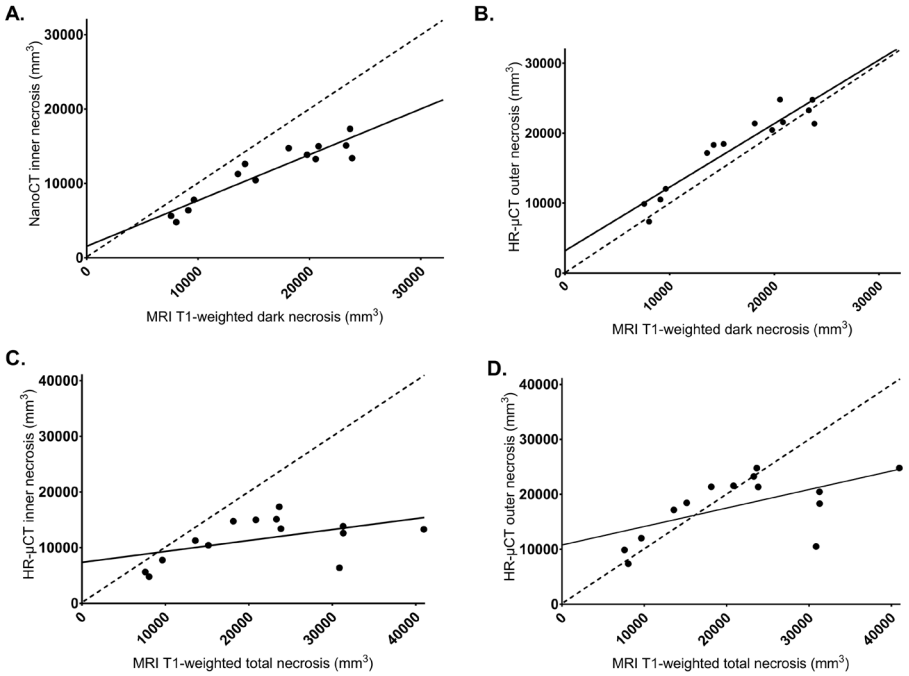

Figure 3. Superposition of T1-weighetd MRI reconstructed volume of dark necrosis (in red) on 3D images of the (A) surface and (B) cut femoral head obtained from HR-µCT. The MRI reconstructed volume delineates the surface where plate micro-cracks are present (A) and (B) includes both the trabecular necrotic and sclerotic zones.

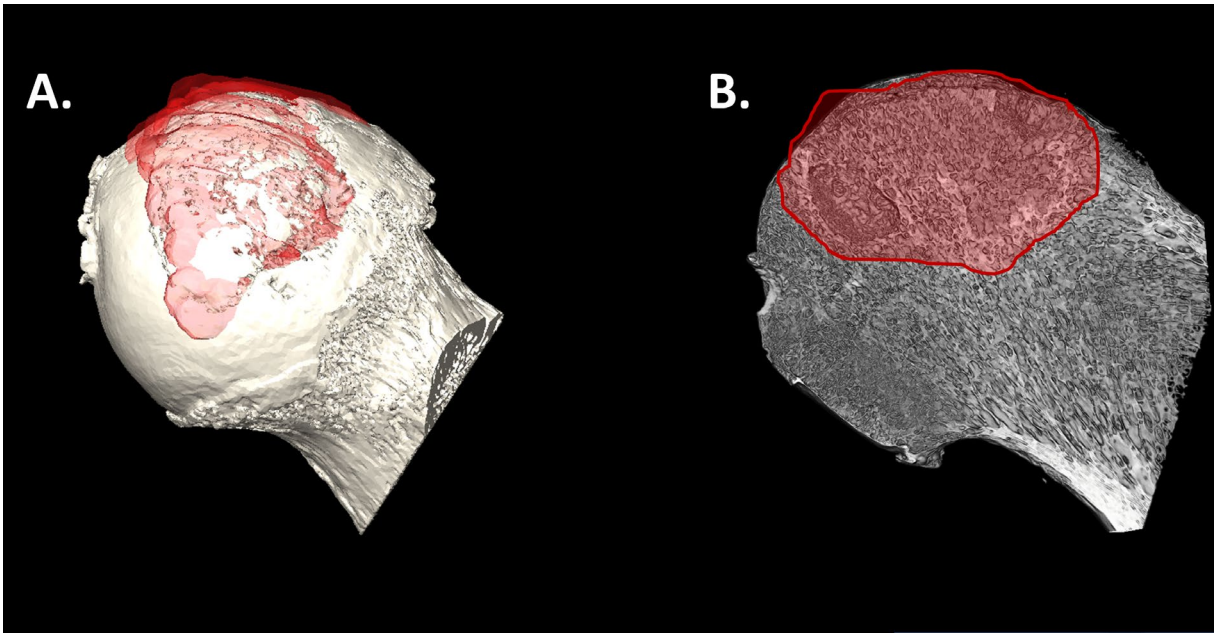

Supplementary Figure. T1-weighted coronal section of a right osteonecrosis of the femoral head. Koo's angle is calculated on the slice with the largest observed necrotic zone. The center of the circle encompassing the femoral head is marked and connected to the two points where the delineation of necrosis intersects the surface of the femoral head. The same angle is calculated on the largest necrosis on a sagittal slice. Koo's index is expressed as a percentage = (coronal angle/180) x (sagittal angle/180) x 100.